Isovector part of optical potentials studied through analog transitions in the (p,n) reaction at 35 MeV

G. C. Jon
Institute of Physics, Academia Sinica, Nankang Taipei, Taiwan 11529

H. Orihara, C. C. Yun, A. Terakawa, K. Itoh, A. Yamamoto, H. Suzuki, H. Mizuno, and G. Kamurai
Cyclotron and Radioisotope Center, Tohoku University, Sendai 980-8578, Japan

K. Ishii
Department of Quantum Science and Energy Engineering, Tohoku University, Sendai 980-8578, Japan

H. Ohnuma
Department of Physics, Chiba Institute of Technology, Narashino-shi, Chiba 275-0023, Japan
(Received 2 November 1999; published 12 September 2000)

Quasielastic (p, n) reactions were studied at an incident proton energy of 35 MeV. Differential cross sections for isobaric analog $\Delta J^{\pi}=0^{+}$ (Fermi-type) transitions and their angular distributions were measured in 27 $N>Z$ target nuclei ^{7}Li, ^{9}Be, ^{13,14}C, ^{15}N, ^{50}Cr, ^{54,56}Fe, ^{58,60,62,64}Ni, ^{70}Zn, ^{71}Ga, ^{92}Zr, ^{110,112,114,115}Cd, ^{116,118,120}Sn, ^{140}Ce, ^{172,174,176}Yb, and ^{208}Pb. Pure $\Delta J^{\pi}=0^{+}$ Fermi-type transitions were observed in 23 of them. As for the four light odd-A nuclei, contributions from mixed $\Delta J^{\pi}\neq 0^{+}$ components were evaluated by microscopic distorted-wave Born approximation (DWBA) calculations to subtract them from the raw data and extract pure Fermi-type transition strengths. Thus 27 $\Delta J^{\pi}=0^{+}$ angular distributions were obtained, and fitted by macroscopic DWBA calculations with the Lane-model optical potential to derive systematically the isovector part of the potential. The best-fit parameters for each target are presented. The present results combined with our previous analysis on 13 other nuclei in the $17\leqslant A\leqslant 48$ region cover almost the entire mass region. They were used to obtain A-dependent global parameters by least-squares fit.

PACS number(s): 25.40.Ep, 27.20.+n, 27.40.+z, 27.50.+e

I. INTRODUCTION

The isospin impurity in nuclei has been a long standing problem in nuclear physics. Studies of isospin symmetry have recently again become a popular subject of nuclear structure physics [1–3], especially due to the development of experimental facilities for charge-exchange reactions and those for radioactive beams. Spreading widths of the isobaric analog states (IAS) give us an important clue to the understanding of the charge-independence-breaking (CIB) and charge-symmetry-breaking (CSB) interactions in nuclei [4–6]. Our recent measurement of the spreading widths of the IAS via the $(p,n_{\mathrm{IAS}}\overline{p})$ reaction and their analysis [7] have revealed that the coupling between the giant isovector monopole state and the IAS induced through the isovector part of the nucleon-nucleus potential is crucial to understand the mass number dependence of the spreading widths of the IAS.

The isovector nucleon-nucleus potential can be derived from optical-model analyses of IAS transitions in the (p,n) reaction, in which transferred total angular momentum and parity ΔJ^{π} are 0^{+}. Such a transition is often called a Fermi-type transition or quasielastic scattering. However, since optical-model analyses suffer from well-known ambiguities in the parameters [8], it is necessary to accumulate data over a wide range of target nuclei as well as over a wide-range of incident energies and carry out systematic analyses. Carlson and collaborators reported a systematic optical model analysis of quasielastic (p,n) reactions at 22.8 MeV on 29 nuclei ranging from ^{9}Be to ^{208}Pb [9]. They derived the isovector potential for each target nucleus, and gave a smooth parametrization of the best-fit parameters for all the nuclei investigated. However, their data and analysis were limited by experimental conditions and theoretical treatment of mixed analog transitions.

We have reported [10] the data and the analysis of isobaric analog transitions at $E_p=35$ MeV in (p,n) reactions on 13 target nuclei in the mass range $17\leqslant A\leqslant 48$. The best-fit parameters for the Lane-type isovector potential were obtained for each transition, and then the mass-number dependence of each parameter was expressed as a linear function of $A^{1/3}$. The strengths of the real part of the Lane potential were determined within $\pm 3\sim\pm 5\,\%$ accuracy in the mass region studied. It was found that imaginary strengths of the Lane potential were almost independent of the mass number.

We have extended our previous work to lighter and heavier target nuclei so that we can study the isovector potential over a wide range of nuclear masses. In this paper we report a study of (p,n) reactions at $E_p=35$ MeV leading to IAS on 27 target nuclei in the regions $7\leqslant A\leqslant 15$ and $50\leqslant A\leqslant 208$; namely, ^{7}Li, ^{9}Be, ^{13,14}C, ^{15}N, ^{50}Cr, ^{54,56}Fe, ^{58,60,62,64}Ni, ^{70}Zn, ^{71}Ga, ^{92}Zr, ^{110,112,114,116}Cd, ^{116,118,120}Sn, ^{172,174,176}Yb, and ^{208}Pb. Analysis similar to our previous work has been made, and the best-fit parameters for the Lane potential were obtained for these nuclei. Combining the present results with our previous results on the *sd*-shell and *f*-shell nuclei [10], we now have a comprehensive set of best-

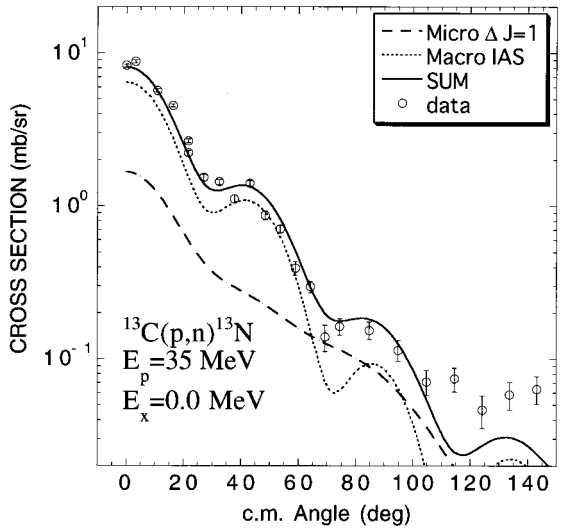

FIG. 1. Differential cross sections for the $^{13}C(p,n)^{13}N$(g.s.) reaction. The dashed line is the result of the microscopic DWBA calculation for the $\Delta J^{\pi}=1^{+}$ component, and the dotted line shows the best-fit result for the $\Delta J^{\pi}=0^{+}$ IAS component. The solid line is the sum of the two.

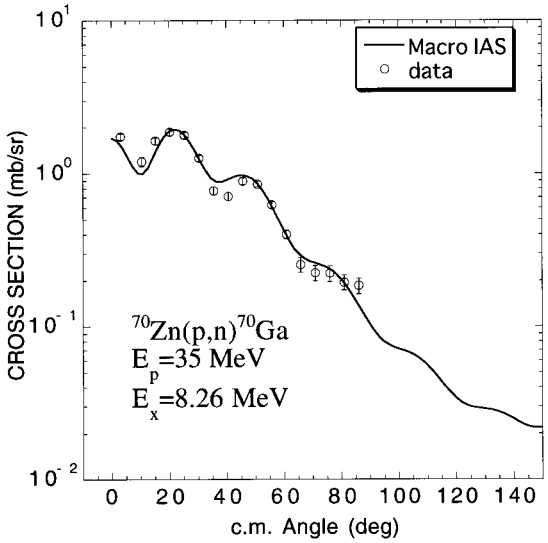

FIG. 2. Differential cross sections for neutrons leading to the 8.26-MeV IAS in ^{70}Zn. This is an example of a pure IAS transition. The solid line shows the macroscopic DWBA calculation obtained with the best-fit parameters obtained for the isovector potential.

fit parameters of the Lane-type isovector potential at $E_p = 35$ MeV. This set was used to extract *A*-dependent global parameters of the Lane potential.

II. EXPERIMENTAL PROCEDURE

The experiment was performed at the Cyclotron and Radioisotope Center, Tohoku University, with a 35-MeV proton beam from an AVF cyclotron and a beam swinger system. The details of the experimental setup have been described previously [11,12]. Neutron energies were measured by the time-of-flight (TOF) technique. The neutron detectors, 23.2 l in a total sensitive volume, were filled with organic liquid scintillator NE213, and located at 44.3 m from the target. The absolute efficiencies of the detectors were obtained from the $^{7}Li(p,n)^{7}Be$ activation analyses with an error less than $\pm 6\%$. Errors in the absolute magnitude of (*p*, *n*) cross sections were estimated to be less than 12%. All the targets were enriched isotopes with enrichments better than 95%, and were self-supporting foil except that gas cells were used for ^{15}N [10,13]. Figures 1, 2, and 3 illustrate the angular distributions of the (*p*,*n*) reactions on ^{13}C, ^{70}Zn, and ^{208}Pb leading to the ground state of ^{13}N and the IAS in ^{70}Ga and ^{208}Bi as representative cases.

III. DWBA ANALYSES

The Lane-model optical potential [14] was used in the macroscopic distorted-wave Born approximation (DWBA) analyses of the quasiscattering data. It is expressed as

$$U(r) = -U_0(r) + (4/A)U_1(r)\vec{t}\cdot\vec{T} + U_{SO}(r) + (1/2 - t_z)V_C(r), \quad (1)$$

where $\vec{t}(\vec{T})$ is the projectile (target) isospin, U_{SO} is the spin-orbit potential, and V_C is the Coulomb potential. The isospin dependent $\vec{t}\cdot\vec{T}$ term yields t_+T_-, t_-T_+, and t_zT_z, corresponding to (*p*,*n*), (*n*,*p*), and (*p*,*p*) or (*n*,*n*) reactions, respectively. The (*p*,*n*) quasiscattering takes place through the term

$$U_{pn}(r) = (2/A)\sqrt{N-Z}\cdot U_1(r). \quad (2)$$

The isovector potential U_1 was parametrized in terms of standard Woods-Saxon forms as

$$U_1(r) = V_1 f(x_R) - 4ia_1 W_1 \frac{d}{dx_1} f(x_1), \quad (3)$$

where

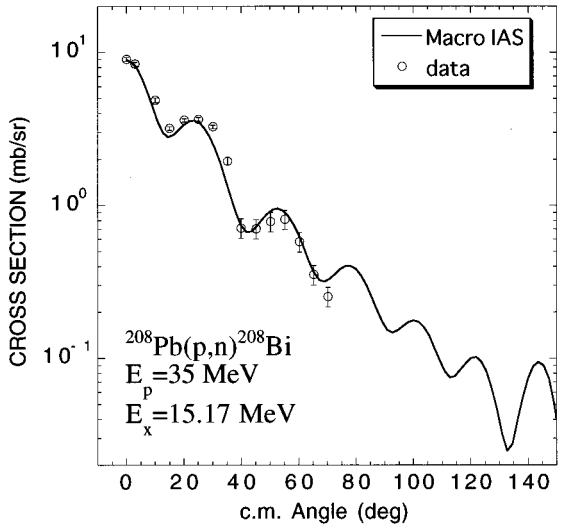

FIG. 3. Same as Fig. 2, but for the 15.17 MeV IAS in ^{208}Pb.

$$f(x)=(1+e^{x})^{-1},$$

$$x=(r-R_i)/a_i,$$

and

$$R_i=r_iA^{1/3}.$$

Here $i=R$ or I. The parameters to be determined are the potential depths V_1 and W_1, geometrical parameters for the real part r_R and a_R, and those for the imaginary part r_I and a_I. To reduce the number of parameters to be fitted, the real geometrical parameters r_R and a_R were fixed to those by Becchetti and Greenless [15]. Then we carried out a parameter search with the program IASEARCH [16] to find the best-fit parameter set to reproduce differential cross sections for each IAS transition.

For the four odd-mass light target nuclei ^{7}Li, ^{9}Be, ^{13}C, and ^{15}N, it was necessary to subtract contributions from $\Delta J^{\pi}\neq 0^{+}$ components. As discussed in detail in Ref. [10], the data in such a case were first compared with microscopic distorted-wave Born approximation (DWBA) results calculated by the computer code DWBA74 [17]. The calculation includes knock-on exchange effects in an exact manner, and thus non-normal parity terms such as $\Delta J(\Delta L,\Delta S)=1(1,0)$ for the $0^{+}\rightarrow 1^{+}$ transition also contribute to the cross section. Optical potential parameters of Becchetti and Greenless [15] were used for the entrance channel. Those for the exit channel were self-consistent potential parameters derived by Carlson *et al.* [9]. The effective nucleon-nucleon interactions (M3Y) by Bertsch *et al.* [18] were used in the microscopic analysis. Spectroscopic amplitudes (OBTD) for the *p*-shell nuclei were obtained from full *p*-shell model calculations using the code OXBASH [19] with the interaction by Millener and Kurath [20]. Single-particle radial wave functions used in DWBA calculations were generated in a Woods-Saxon potential with $r_0=1.25$ fm, $a=0.6$ fm, $V_{LS}=6$ MeV, and the depth adjusted to reproduce the binding energy of a valence nucleon. The calculated cross sections for the $\Delta J^{\pi}\neq 0^{+}$ components were subtracted from the raw data to extract cross sections for the pure $\Delta J^{\pi}=0^{+}$ Fermi-type transition. The DWBA results for the $C^{13}(p,n)N^{13}$ (g.s.) are shown in Fig. 1 as an example. This is a $\frac{1}{2}^{-}\rightarrow\frac{1}{2}^{-}$ transition and two ΔJ^{π} values 0^{+} and 1^{+} are allowed. Therefore the cross sections for the $\Delta J^{\pi}=1^{+}$ component were calculated microscopically and subtracted from the data, and the Lane potential parameters were fitted to the rest.

Sensitivity of such microscopic calculations to the parameters involved and reliability of the derived conclusions are elaborated in Ref. [21]. As for the quasielastic and inelastic scattering, a macroscopic calculation usually gives a better description of the data than a microscopic calculation [22,13]. As discussed in Ref. [22], this is primarily because numerous minor transition amplitudes arising from many-particle many-hole configurations contribute coherently to the quasiscattering while a shell-model calculation within a limited model space can give only major amplitudes. For transitions other than quasiscattering, on the other hand, minor components add up incoherently and cancel out, or they come into the transition only through higher-order processes. Therefore microscopic DWBA calculations usually give good descriptions of the transitions other than quasielastic as shown in our many previous samples [21,22,13].

Table I lists the best-fit parameters for each reaction together with those for *sd*- and *f*-shell nuclei obtained in Ref. [10]. The radius of the imaginary potential decreases gradually, while the diffuseness parameter increases, as the mass number increases. The real potential depth V_1 also increases with the mass number. All of them seem to have linear dependence on $A^{1/3}$. The imaginary potential depth W_1, on the other hand, is almost constant in the mass region studied. These best-fit parameters are plotted as a function of $A^{1/3}$ in Figs. 4 and 5. It should be noted that the values obtained from the ''subtracted data'' for odd-*A* light target nuclei lie on a smooth line, confirming the validity of the procedure described above and reliability of microscopic calculations. The solid lines indicate results of least-squares fit assuming that each parameter is a linear function of $A^{1/3}$. Taking the diagonal and off-diagonal elements of the error matrices [23], we were able to describe $A^{1/3}$ dependence of the potential parameters as

$$V_1=6.38+2.25A^{1/3}\pm\sqrt{0.39-2\times 0.094A^{1/3}+0.024A^{2/3}}, \tag{4}$$

$$W_1=5.09+0.39A^{1/3}\pm\sqrt{0.22-2\times 0.058A^{1/3}+0.016A^{2/3}}, \tag{5}$$

and

$$r_I=1.98-0.15A^{1/3}\pm\sqrt{0.0037-2\times 0.0010A^{1/3}+0.0002A^{2/3}}, \tag{6}$$

$$a_I=-0.090+0.22A^{1/3}\pm\sqrt{0.0020-2\times 0.0005A^{1/3}+0.0002A^{2/3}}. \tag{7}$$

The dotted and dash-dotted lines in Figs. 4 and 5 indicate values one standard deviation above and below the best-fit value, respectively. The results obtained in Ref. [10] for *sd*- and *f*-shell nuclei are overlaid by thick lines for comparison.

IV. DISCUSSION

As discussed in Ref. [10], only minor effects were observed for the feedback of the finally obtained potential to the microscopic DWBA calculations and to the distorted waves in the entrance and exit channels in the macroscopic DWBA analysis. These correction terms are $\pm U_1(N-Z)/A$ for the neutron and proton channels, respectively, and only a few percent of the distorting potential strengths at most. Some of the data were reanalyzed by using the finally obtained optical potential parameters. Negligibly small contributions from the correction terms were found, and the results in the previous section are hardly changed.

The thick lines obtained from a ''local'' analysis for *sd*- and *f*-shell nuclei in Ref. [10] coincide in the region $A^{1/3}=2.6-3.6$ with the present results of the ''global'' analysis. However, we have weaker $A^{1/3}$ dependence of the geometrical parameters in the global analysis than in the local analysis.

The present results are in general agreement with those in

TABLE I. Best-fit parameters of isovector potential for each nucleus.

Reaction	$E_{\rm exc}$ of IAS (MeV)	V_1 (MeV)	W_1 (MeV)	r_I (fm)	a_I (fm)
^{7}Li$(p,n)^{7}$Be	0.0	11.7±1.6	5.6±1.1	1.92±0.07	0.39±0.07
^{9}Be$(p,n)^{9}$B	0.0	12.5±1.1	6.4±0.9	1.78±0.06	0.42±0.05
^{13}C$(p,n)^{13}$N	0.0	12.4±1.1	6.2±0.8	1.70±0.06	0.46±0.05
^{14}C$(p,n)^{14}$N	2.3129	13.2±1.1	6.6±0.8	1.75±0.05	0.46±0.05
^{15}N$(p,n)^{15}$O	0.0	11.6±1.0	6.3±0.8	1.73±0.06	0.41±0.05
^{17}O$(p,n)^{17}$F	0.0	12.0±1.3	6.0±0.8	1.75±0.05	0.45±0.05
^{18}O$(p,n)^{18}$F	1.041	11.3±1.1	5.8±0.6	1.56±0.04	0.45±0.05
^{22}Ne$(p,n)^{22}$Na	0.657	12.2±0.7	5.6±0.6	1.60±0.05	0.45±0.06
^{25}Mg$(p,n)^{25}$Al	0.0	12.1±1.6	6.2±0.9	1.58±0.07	0.50±0.07
^{26}Mg$(p,n)^{26}$Al	0.228	12.7±0.6	6.3±0.4	1.54±0.03	0.53±0.04
^{27}Al$(p,n)^{27}$Si	0.0	11.0±1.5	5.9±1.0	1.40±0.06	0.50±0.07
^{30}Si$(p,n)^{30}$P	0.677	11.8±1.2	6.5±0.3	1.49±0.03	0.53±0.03
^{34}S$(p,n)^{34}$Cl	0.0	12.9±0.8	6.2±0.6	1.43±0.03	0.58±0.05
^{38}Ar$(p,n)^{38}$K	0.130	13.3±0.9	6.5±0.5	1.40±0.02	0.67±0.03
^{40}Ar$(p,n)^{40}$K	4.384	14.0±0.6	5.9±0.3	1.37±0.02	0.72±0.03
^{42}Ca$(p,n)^{42}$Sc	0.0	13.2±0.5	6.7±0.5	1.41±0.03	0.70±0.03
^{44}Ca$(p,n)^{44}$Sc	2.783	15.6±1.0	7.7±1.0	1.41±0.05	0.70±0.05
^{48}Ca$(p,n)^{48}$Sc	6.677	13.9±0.9	6.4±0.8	1.40±0.03	0.72±0.03
^{50}Cr$(p,n)^{50}$Mn	0.0	12.5±1.0	5.6±0.8	1.30±0.08	0.80±0.10
^{54}Fe$(p,n)^{54}$Co	0.0	15.8±0.7	7.2±0.7	1.32±0.09	0.91±0.07
^{56}Fe$(p,n)^{56}$Co	3.5	15.0±0.9	6.8±0.8	1.45±0.08	0.87±0.06
^{58}Ni$(p,n)^{58}$Cu	0.203	15.0±1.0	7.4±0.9	1.37±0.07	0.88±0.06
^{60}Ni$(p,n)^{58}$Cu	2.54	14.4±0.9	6.7±0.8	1.41±0.07	0.88±0.05
^{62}Ni$(p,n)^{58}$Cu	4.63	16.4±0.8	7.4±0.8	1.37±0.07	0.91±0.04
^{64}Ni$(p,n)^{58}$Cu	6.71	16.5±1.2	7.4±0.8	1.38±0.09	0.89±0.06
^{70}Zn$(p,n)^{70}$Ga	8.26	15.6±1.2	4.9±1.7	1.37±0.09	0.95±0.17
^{71}Ga$(p,n)^{71}$Ge	8.96	17.2±1.8	7.0±1.2	1.40±0.13	0.83±0.15
^{92}Zr$(p,n)^{92}$Nb	8.94	14.9±1.8	5.9±1.0	1.23±0.10	0.91±0.08
^{110}Cd$(p,n)^{110}$In	8.80	16.7±0.9	5.7±0.7	1.36±0.09	0.97±0.07
^{112}Cd$(p,n)^{112}$In	10.04	17.1±1.0	8.0±0.9	1.19±0.14	1.05±0.15
^{114}Cd$(p,n)^{114}$In	11.12	16.3±0.9	6.4±0.8	1.34±0.08	0.95±0.06
^{116}Cd$(p,n)^{116}$In	12.04	16.8±0.9	6.7±0.9	1.36±0.07	0.98±0.05
^{116}Sn$(p,n)^{112}$Sb	8.61	18.3±0.9	6.0±1.2	1.28±0.10	1.10±0.12
^{118}Sn$(p,n)^{118}$Sb	9.36	16.4±0.8	6.6±0.7	1.34±0.09	0.97±0.05
^{120}Sn$(p,n)^{120}$Sb	10.24	16.9±0.9	7.0±1.0	1.35±0.10	0.98±0.07
^{140}Ce$(p,n)^{140}$Pr	11.04	18.8±1.3	7.6±1.0	1.18±0.09	1.05±0.05
^{172}Yb$(p,n)^{172}$Lu	13.7	19.3±0.9	8.1±0.9	1.31±0.08	1.12±0.13
^{174}Yb$(p,n)^{174}$Lu	14.8	18.9±0.8	7.9±1.0	1.18±0.09	1.19±0.10
^{176}Yb$(p,n)^{176}$Lu	16.0	19.0±1.0	7.0±1.0	1.27±0.10	1.00±0.10
^{208}Pb$(p,n)^{208}$Bi	15.17	19.9±1.0	7.4±1.5	1.12±0.05	1.28±0.08

Ref. [9] at $E_p = 22.8$ MeV. There are some differences, however, probably due partly to the incident-energy dependence of the potential and partly to a different analysis method. The imaginary depth of the isovector potential W_1 was fixed at $W_1/V_1 = \frac{1}{2}$ in Ref. [9], while it was taken as a free parameter in the present analysis. As seen in Fig. 4, W_1 shows a different mass-number dependence from V_1. It is almost constant and about 6 MeV over the whole mass region studied. Furthermore, the present values for the geometrical parameters r_I and a_I show weaker $A^{1/3}$ dependence. The mass number dependence of the radius parameter r_I was $-0.4A^{1/3}$ in Ref. [9] and $-0.258A^{1/3}$ in Ref. [10] for *sd*- and *f*-shell nuclei only, while it is $-0.15A^{1/3}$ in the present analysis. Similarly, that for a_I was $0.46A^{1/3}$ in Ref. [9], $0.312A^{1/3}$ in Ref. [10], and $0.22A^{1/3}$ in the present analysis, respectively. The magnitudes of V_1 obtained here are about 20% smaller than those obtained by Carlson *et al.*

To summarize, we have extended our previous study [10] of the isovector part of the optical potential to a total of 40 nuclei. Analog transitions have been observed in (p, n) reactions at $E_p = 35$ MeV on 27 target nuclei ranging $7 \leqslant A \leqslant 15$ and $50 \leqslant A \leqslant 208$. Pure $\Delta J^{\pi} = 0^{+}$ Fermi-type transitions were

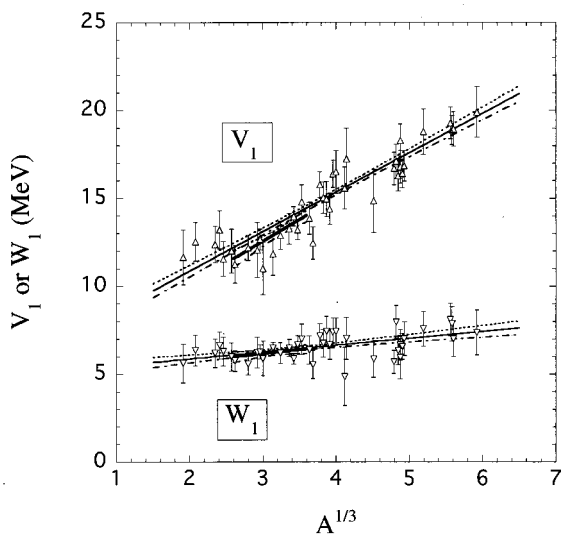

FIG. 4. Best-fit values of V_1 and W_1 plotted as a function of $A^{1/3}$. The solid lines indicate results of least-squares fit with errors shown by the dotted $(+\sigma)$ and dot-dashed $(-\sigma)$ lines calculated from error matrices.

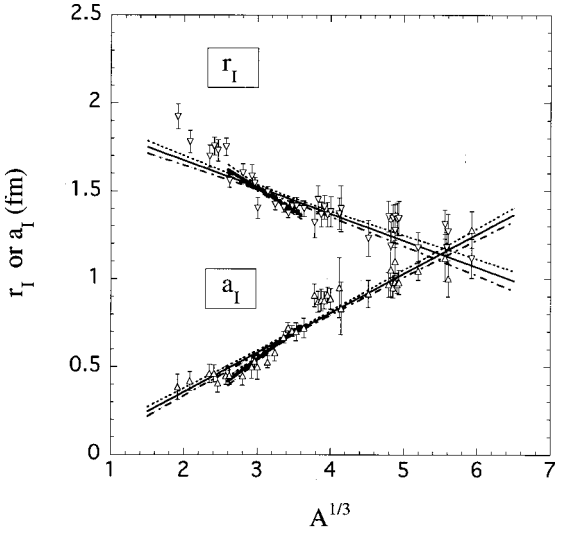

FIG. 5. Same as Fig. 4 but for r_1 and a_1.

observed for nuclei in $50 \leqslant A \leqslant 208$. As for the light odd-mass nuclei, contributions from mixed $\Delta J^{\pi} \neq 0^{+}$ components were evaluated by microscopic DWBA calculations to subtract them from the raw data and extract pure Fermi-type transition strengths. The best-fit parameters for the Lane-type isovector potential (V_1, W_1, r_I, a_I) were obtained for each transition. Combining the results with our previous results on 13 *sd*- and *f*-shell nuclei, we have obtained 40 parameter sets, which cover almost the entire mass region. These parameters were expressed as a linear function of $A^{1/3}$. The values of V_1 were determined by present parametrization within $\pm 2 \sim \pm 4$ % accuracy in the mass region studied. Our previous conclusion [10] that W_1 is almost independent of $A^{1/3}$ was confirmed.

The present analysis gives the most extensive result of the Lane-type isovector nucleon-nucleus potential at 35 MeV, and hopefully future work at different energies will enable us to study not only mass dependence but also energy dependence of the isovector potentials.

ACKNOWLEDGMENTS

One of the authors (H.Oh.) acknowledges partial financial support by The Ministry of Education, Science, Sports and Culture under Grant-in Aid for Scientific Research (C) No. 09640371. One of the authors G.C.J. is indebted to Professor E. K. Lin for his support of this work.

[1] I. Hamamoto and H. Sagawa, Phys. Rev. C **48**, R960 (1993).
[2] H. Sagawa, Nguyen van Giai, and T. Suzuki, Phys. Lett. B **353**, 7 (1995).
[3] T. Suzuki, H. Sagawa, and G. Colò, Phys. Rev. C **54**, 2954 (1996).
[4] T. Suzuki, H. Sagawa, and N. Van Giai, Phys. Rev. C **47**, R1360 (1993).
[5] G. Colò and Nguyen van Giai, Phys. Rev. C **53**, 2201 (1996).
[6] U. Van Kolck, J. L. Friar, and T. Goldman, Phys. Lett. B **271**, 169 (1996).
[7] H. Orihara *et al.*, Phys. Rev. Lett. **81**, 3607 (1998).
[8] For example, P. E. Hodgson, *Growth Points in Nuclear Physics* (Pergamon, Oxford, 1981), Vol. 3.
[9] J. D. Carlson, C. D. Zafiratos, and D. A. Lind, Nucl. Phys. **A249**, 29 (1975).
[10] G. C. Jon *et al.*, Phys. Rev. C **56**, 900 (1997).
[11] H. Orihara and T. Murakami, Nucl. Instrum. Methods **181**, 15 (1981).
[12] H. Orihara *et al.*, Nucl. Instrum. Methods Phys. Res. A **257**, 189 (1987).
[13] M. Oura *et al.*, Nucl. Phys. **A586**, 20 (1995).
[14] A. M. Lane, Phys. Rev. **8**, 171 (1962).
[15] F. D. Becchetti and G. W. Greenless, Phys. Rev. **182**, 1190 (1969).
[16] A parameter search code for elastic and quasielastic scattering. Quasielastic calculations are made using the Lane model and adopted from the code DWUCK4 originally written by P. D. Kunz.
[17] R. Schaeffer and J. Raynal, Centre d'Etude Nucleaires de Saclay Report No. CEA-R4000, 1970.
[18] G. Bertsch *et al.*, Nucl. Phys. **A284**, 399 (1977).
[19] A. E. Echegoyen *et al.*, National Superconducting Cyclotron Laboratory Report No. 524, 1984.
[20] D. J. Millener and D. Kurath, Nucl. Phys. **A255**, 315 (1975).
[21] H. Ohnuma *et al.*, Nucl. Phys. **A467**, 61 (1987).
[22] K. Furukawa *et al.*, Phys. Rev. C **36**, 1686 (1987).
[23] M. Fujioka, CYRIC annual report, 1995, p. 54. The full report is available at URL http://www.cyric.tohoku.ac.jp/english/report/repol995/95p15.pdf